Coherent combining of low-power optical signals based on optically amplified error feedback

Research Article Vol. 30, No. 11 / 23 May 2022 / Optics Express 19441
Optics EXPRESS

Coherent combining of low-power optical signals based on optically amplified error feedback

RASMUS LARSSON,* JOCHEN SCHRÖDER, MAGNUS KARLSSON, AND PETER A. ANDREKSON

Photonics Laboratory, Department of Microtechnology and Nanoscience, Chalmers University of Technology, SE - 412 96 Gothenburg, Sweden
*rasmus.larsson@chalmers.se

Abstract: In free-space optical communication links, the combining of optical signals from multiple apertures is a well-known method to collect more power for improved sensitivity or mitigation of atmospheric disturbances. However, for analog optical combining no detailed analysis has been made in cases when the optical signal power is very low (<−60 dBm) as would be the case in very long-haul free-space links. We present a theoretical and experimental study of analog coherent combining of noise-limited signals from multiple independent apertures by applying low frequency optical phase dithering to actively compensate the relative phases. It is experimentally demonstrated that a 97% combining efficiency of four 10 GBaud QPSK signals is possible with a signal power per aperture exceeding −80 dBm, in fair agreement with theory. We also discuss the scaling aspects to many apertures.

1. Introduction

For the past few decades the main implementations of space communications, be it inter-satellite, satellite to ground or deep space links, have relied on radio and microwave frequencies for transmission. Aside from this well-established technique, a growing interest in the use of shorter wavelengths is emerging in this research field [1]. Due to diffraction, transmission of shorter wavelength radiation promise higher data rates and reduced propagation losses [2]. Thus it comes as no surprise that many recent investigations [3–5] have begun targeting free space optical (FSO) communication links.

A recent, successful demonstration of a laser communication link between a satellite in lunar orbit, with a 15 cm transmit aperture, and a ground station on earth, with four 40 cm receive apertures, was reviewed in [6]. Moreover, regarding reception of weak optical signals a sensitivity of 0.5 photons per bit (ignoring coupling losses) using photon counting nano-wire detector arrays was demonstrated in [7]. These systems rely on the detected power of the signal and are therefore considered incoherent in their implementation.

Looking to the increasing maturity of optical fiber-based communication links, it is clear that the gains of its technological transition to coherent techniques is aspiring to the area of free space optical communications. The benefit of coherent detection lies in the recovery of both signal phase and amplitude. This allows for higher data rate, sensitivity and acquisition of additional information in light based measurements [8]. Evidently, be it in context of data transmission or other metrology applications such as LIDAR, this advancement in technology is appealing.

However, for coherent applications, difficulties arise when climbing the frequency ladder in the electromagnetic spectrum. Pertaining to the small wavelengths of light, system components dealing with transmission and collection of optical signals need to be manufactured with a

#456188 https://doi.org/10.1364/OE.456188
Journal © 2022 Received 16 Feb 2022; revised 10 Apr 2022; accepted 12 Apr 2022; published 18 May 2022

Optics EXPRESS

corresponding accuracy for efficient recovery of the phase. Therefore, an important aspect of reception of electromagnetic signals is the effective collection area which is proportional to the end received power.

While for receiving architectures of incoherent signals, it is relatively straightforward to accomplish larger detection areas, this does not hold for coherent approaches. At the receiver side, many current optical systems employ a monolithic telescope that focuses incoming light onto a photo-detector. Manufacturing imperfections of the telescope as well as turbulence in the transmission medium lead to aberrations in the received optical wavefront, which severely impedes the phase acquisition.

Several attempts at mitigating this issue have been investigated. A common technique comprises the utilisation of a high precision manufactured telescope alongside a deformable mirror for adaptive optical wavefront correction [9–11]. The cost of manufacture of these large area high precision telescopes increases rapidly with size however [12]. In a space environment they are also prone to deformation because of temperature changes which further distorts the wavefront.

A different approach towards a larger receive area is that of an array of multiple smaller and cheaper apertures that individually couple light into single mode optical fibers (SMFs). Detection at separate receive apertures may provide spatial information or can provide averaging that mitigates outages in the case of channel fading due to atmospheric turbulence [13,14]. For the purpose of detecting weak optical signals however, the output of the individual single mode fibers can be combined coherently to provide a larger received signal.

To date, concerning coherent combining of single mode signals, two different approaches have been investigated. A visualisation of the two is depicted in Fig. 1.

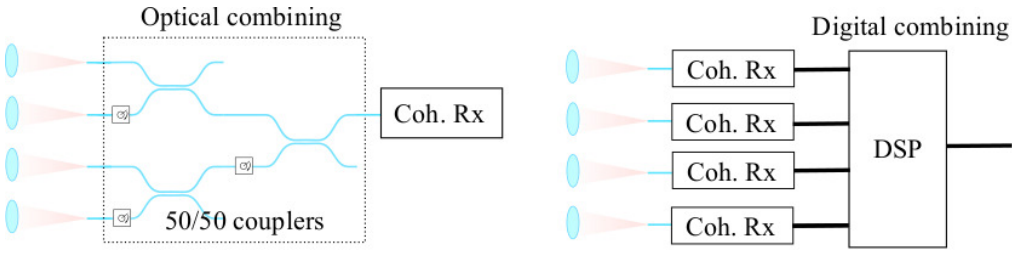

Fig. 1. Left: a schematic of an optical combining architecture. Four individual receive channels are combined and detected using a coherent receiver (Coh. Rx). Right: a schematic of a digital combining architecture. Four separated channels are individually detected using coherent receivers before subsequent digital combining using digital signal processing (DSP).

The analog approach in which the signals are combined in the optical domain require phase, amplitude and polarisation to be aligned optically before combining. Any instability in the free space transmission channel (turbulence) or receiver (temperature changes, vibrations or pointing errors) will induce fluctuations in these parameters. In practice however, phase fluctuations pose the most severe degradation [15] and have been the focus of recent investigations [15–18]. Furthermore, for deep space links where ultimate sensitivity is of interest there is no turbulent medium which may scramble amplitude and polarisation to such degree as to uncorrelate them between receive apertures. For these applications it is safe to assume phase fluctuations is the major problem in need of compensation, provided that tip and tilt control of alignment optics is already carried out. This is in general a reasonable assumption since alignment tracking and compensation at long distances can be slow. While this approach has to align the electromagnetic field between channels and combat optical loss in the combining architecture, it provides a

Optics EXPRESS

combined signal available for further optical processing. Such processing could furthermore improve the signal reception, as demonstrated by [19].

In digital combining, separate signals are individually coherently detected at their respective coherent receivers. There is thus no need to worry about amplitude mismatch. Phase, polarisation and possible channel delays between channels are instead matched digitally. It has been shown in [20] that an impressive 100% digital combining efficiency for as low as 0.03 photons per bit per aperture (corresponding to −70.9 dBm at 10 Gbaud quadrature phase shift-keying) for offline digital signal processing (DSP) is possible. However, the estimation of phase and delay is a complex and energy-inefficient task for the DSP, which recent investigations [21–23] have studied. For instance, [22] notes that practical real-time digital combining suffers a reduction in efficiency for weak signals. The need for a coherent receiver for each channel also implies a high cost and complexity when scaling up to a large number of channels.

As for analog combining, while promising results have been demonstrated at high signal to noise ratio (SNR), there is still a lack of studies exploring the low-SNR limit. Specifically, how weak optical signals can be coherently combined and how such a system scales to a larger number of channels is of practical interest.

To investigate this we have built an analog phase compensating system targeting coherent combining of low-SNR optical signals. The system architecture is based on pairwise combining of channels using 50/50-couplers. The active control system responsible for phase error tracking and compensation at each stage performs optical preamplification of the phase dither error signal for feedback. Two and four aperture combining of a quadrature phase shift-keyed (QPSK) signal is studied at low power and for different phase fluctuations strengths. From these investigations an extrapolating prediction of system performance under different external conditions, i.e., fluctuation strength, received signal power, optical bandwidth and number of channels is discussed.

Section 2 introduces the optical combining stage and outlines the operation of the control system used. The performance of the system is theoretically discussed in terms of the phase dithering and the impact of noise, phase fluctuations, signal bandwidth and up-scaling are addressed. Section 3 describes the experimental measurements and setup. In section 4 we discuss the performance of the single combining stage in terms of measurements and simulation and apply the theory to make generalised performance predictions at a range of different received powers and phase fluctuation strengths. Section 5 addresses up-scaling to multiple channels and the work is discussed and concluded in section 6.

2. Control system

Here we present the 2-channel combining stage and its corresponding control system for mitigating phase fluctuations.

The 2-channel combining stage is depicted in Fig. 2. A polarization controller (PC) in the upper arm matches the polarization of the two inputs. In the lower arm the light passes through a piezoelectric transducer (PZT), which via a feedback loop attempts to compensate the relative phase fluctuation ϕ. It does so by modulating the phase (optical path length) of the present channel through the phase factor $\phi_{\mathrm{PZT}} = -\phi_{\mathrm{DC}} + \phi_{\mathrm{dither}}$ where, ideally, $\phi_{\mathrm{DC}} = \phi$ and ϕ_{dither} is used to generate the control system error signal. The output powers are

$$P_1 = P_s[1 - \cos(\phi + \phi_{\mathrm{PZT}})], \quad P_2 = P_s[1 + \cos(\phi + \phi_{\mathrm{PZT}})]. \tag{1}$$

Here, $P_s \propto |E_s|^2$ is the average optical power per aperture, that is, per input to the 50/50-coupler.

The phase dither applied in the PZT can be written as $\phi_{\mathrm{dither}}(t) = \phi_{\mathrm{mag}} \cos(2\pi f_{\mathrm{dither}} t)$ where f_{dither} is the dither frequency and ϕ_{mag} is the magnitude. The dither frequency must be chosen large enough such that the dither is too fast for the control system to react on.

The phase dither produces a component of P_1 oscillating at frequency f_{dither} which is detected in the power detection stage, filtered and amplified by the low noise amplifier (LNA) before being

Optics EXPRESS

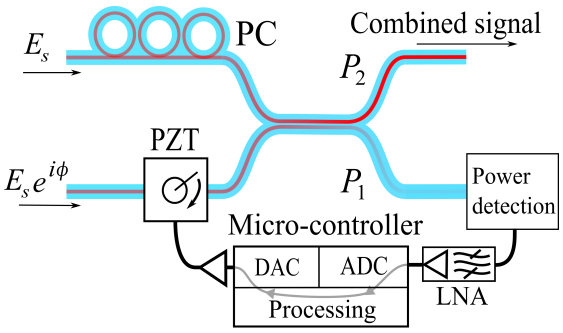

Fig. 2. A single combining stage. E_s denote the complex electric field and ϕ the relative phase fluctuation. PZT: piezoelectric transducer, PC: polarisation controller, LNA: low noise amplifier, ADC: analog to digital converter, DAC: digital to analog converter.

digitised and processed in the micro-controller. The processing comprises digital signal bandpass filtering with a narrow filter bandwidth Δf centered at f_{dither} and in-phase demodulation. The resulting baseband error signal is

$$s(t) = K_C P_s \phi_{\text{mag}} \sin \phi_e(t-\tau) + n(t). \tag{2}$$

Here, K_C is a constant that accounts for detection and processing steps carried out on the error signal, t is the time, τ is the loop delay, n is the dominating noise remaining on the processed signal and $\phi_e = \phi - \phi_{\text{DC}}$ is the phase error, i.e. the residual relative phase after the PZT.

To minimise the residual error ϕ_e (and thereby maximise the combined power) the DC phase offset provided by the PZT is updated based on the processed error signal according to

$$\phi_{\text{DC}}(M\Delta t) = \phi_{\text{DC}}\big((M-1)\Delta t\big) + \phi_{\text{step}}\text{sgn}\big(s(t)\big) \tag{3}$$

where M is an integer, ϕ_{step} ($\pi \gg \phi_{\text{step}} > 0$) is the fixed phase update step per time interval $\Delta t = 1/f_{\text{dither}}$ and $\text{sgn}(x)$ denotes the sign-function. Provided this choice, ϕ_e will be minimised.

The combining efficiency (excluding component excess losses), defined for a single 2-channel combining stage, is

$$\eta = \frac{P_2}{P_1 + P_2} \tag{4}$$

where $\eta = 1$ corresponds to perfect coherent combining while $\eta = 1/2$ is the case of incoherent combining. Hence we will use η as a measure of system performance from here on.

While high η is achievable using this system some penalties will remain. Due to the dither and loop delay-induced oscillation, the maximum attainable time-average combining efficiency (neglecting noise and phase fluctuations) is theoretically limited to (see Supplement 1 sect. 1A)

$$\bar{\eta} = \frac{1}{2}\left[1 + J_0(\phi_{\text{mag}})\text{sinc}\left(\frac{\phi_{\text{step}} f_{\text{dither}}}{2\Delta f}\right)\right] \tag{5}$$

where $J_0(x)$ is the Bessel function of the first kind and $\text{sinc}(x) = \sin(x)/x$. Here the loop delay is further assumed to be limited by the filtering ($\tau \approx 1/2\Delta f$).

For most of our investigation here, the sinc-factor is approximately 1 due to the choice of small ϕ_{step}. In this case the fixed step update approach of Eq. (3) will perform similarly to an error signal-proportional gradient descent-approach: $\Delta\phi_{\text{DC}}(t) \propto s(t)$. Meanwhile, the benefit of the fixed step update approach is its insensitivity to fluctuations in the received power per aperture P_s which may cause instability if $\Delta\phi_{\text{DC}}(t) \propto s(t)$.

Optics EXPRESS

2.1. External limitations

Other than the internal system limitations above, external conditions put forward requirements and limitations as well. The system needs to be sufficiently fast to cope with the phase fluctuations it is subject to while also produce a strong enough error signal that does not drown in noise.

Starting with the system speed limitation, a practical measure of the strength of the phase fluctuation $\dot{\phi} = \frac{d\phi}{dt}$ is given by its standard deviation $\sigma_{\dot{\phi}}$. The speed requirement on the system to maintain high combining efficiency becomes

$$\alpha\sigma_{\dot{\phi}} \leq \phi_{\text{step}} f_{\text{dither}}. \tag{6}$$

This assumes zero average phase change ($\langle\dot{\phi}\rangle$=0) which is expected from a random phase variation. The factor α will depend on the exact statistical properties of $\phi(t)$ as well as our tolerance on η. Equation (6) is the system speed limit criterion which at equality describes the maximum fluctuation strength the system can handle. Note that the relation between $\sigma_{\dot{\phi}}$ and common atmospheric turbulence parameters is non-trivial and depends on aperture size and separation. If the atmospheric time constant t_a is defined with a significant phase change of 1 radian then the maximum phase fluctuation strength the turbulence can cause can be estimated as $\sigma_{\dot{\phi}} \lessapprox 1\text{radian}/t_a$, where typically t_a>1 ms [24].

In terms of noise, for direct power detection of very weak optical signals, thermal noise will dominate (ignoring background illumination and dark current). Hence we use an erbium doped fiber amplifier (EDFA) as preamplifier to improve SNR, see Fig. 3.

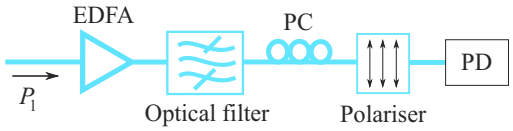

Fig. 3. The power detection stage of the optical error signal. EDFA: erbium doped fiber amplifier, PD: photo-detector.

The Power P_1 is fed into an EDFA followed by, a narrow optical bandpass filter of bandwidth $\Delta\nu$, a PC aligning the signal polarisation to the subsequent polariser before detection in a photo-detector. By introducing optical amplifiers, in our case EDFAs, the dominant noise is given by the spontaneous-spontaneous ($\sigma^2_{\text{sp-sp}}$) beat-noise term arising in a square-law detector [25]. This holds as long as the amplified spontaneous emission (ASE) noise power, neglecting the gain, (which is > -61 dBm at a bandwidth of 0.1 nm) is larger than P_1. Furthermore, by implementing the polariser $\sigma^2_{\text{sp-sp}}$ is halved.

After photo detection the spontaneous-spontaneous beat noise is filtered and processed along with the signal and will influence with which sign ($\pm\phi_{\text{step}}$) ϕ_{DC} is updated based on the SNR of s from Eq. (2). If the step size ϕ_{step} is made smaller and smaller, then the time it takes for the system to update ϕ_{DC} e.g. a full radian ($t_{1\text{rad}}$) will increase ($t_{1\text{rad}} = \Delta t \cdot 1\text{rad}/\phi_{\text{step}}$), if the update frequency is fixed. This is similar to averaging the signal s over an equally long time before taking a full 1 radian step in ϕ_{DC}. To account for this averaging of the signal we will instead of looking at the SNR of s from Eq. (2) consider the energy per 1 radian step to noise power spectral density ratio: $E_{1\text{rad}}/N_0 = \text{SNR} \cdot t_{1\text{rad}}\Delta f$, defined for $\sin^2\phi_e$ averaged to 1/2 and $\Delta f \gg 1/t_{1\text{rad}}$ (for derivation see Supplement 1 sect. 1B)

$$E_{1\text{rad}}/N_0 = \frac{2P_s^2\phi_{\text{mag}}^2}{(F_n h\nu)^2\phi_{\text{step}} f_{\text{dither}}(\Delta\nu - \Delta f/2)}. \tag{7}$$

Here F_n is the EDFA noise figure, h Planck's constant and ν the optical frequency.

Optics EXPRESS

Reasonably, $E_{1\mathrm{rad}}/N_0$ needs to be large enough for the system to maintain a high η. We define the noise limit criterion via the $(E_{1\mathrm{rad}}/N_0)_{\mathrm{thr}}$ such that $E_{1\mathrm{rad}}/N_0 \geq (E_{1\mathrm{rad}}/N_0)_{\mathrm{thr}}(\eta)$, where the exact threshold value will depend on the system and what η we require. This condition is from here on referred to as the noise limit criterion of the combining system which at equality determines the minimum received power per aperture P_s we require, i.e. the system sensitivity.

The two external conditions (noise and phase fluctuations) lead to a trade-off between bandwidth and sensitivity. By using Eq. (6) at equality to substitute $\phi_{\mathrm{step}}f_{\mathrm{dither}}$ in Eq. (7) and $\Delta f \ll \Delta\nu$ we reach a combined criterion that considers both of these conditions and is given as

$$\frac{P_s^2}{\sigma_{\dot{\phi}}\Delta\nu} \geq K, \quad K \approx (E_{1\mathrm{rad}}/N_0)_{\mathrm{thr}}\frac{\alpha(F_n h\nu)^2}{2\phi_{\mathrm{mag}}^2}. \tag{8}$$

Note that the optical filter bandwidth can be minimised to the optical signal bandwidth $\Delta\nu_s$.

Equation (8) tells us that if the input power per aperture, optical signal bandwidth or the phase fluctuation strength changes the following relation must be kept for equal system combining efficiency: $P_s^2 \propto \sigma_{\dot{\phi}}\Delta\nu_s$. The constant K may be decreased by increasing ϕ_{mag} but due to the penalty to η predicted by Eq. (5) the usefulness of doing so is limited. This implies that the system cannot work for combinations of too low received powers and too strong phase fluctuations at a fixed signal bandwidth.

2.2. Simulating the control system

Time domain simulations of the control system were performed for comparison with the experimental results. These simulation results are presented alongside the experimental 2-channel results in sect. 4. The simulations are based on the same digital processing carried out by the micro-controller. The random phase fluctuation (generated as pink noise) was added to the input field along with the phase modulation of the PZT. The 50/50 coupler was modelled using its analytical transfer equations and the output fields are detected using a square law detector-model. The dominant noise power was calculated from $\sigma^2_{\text{sp-sp}}$ in [25] with EDFA noise figure $F_n = 3.6$ dB and used to scale the white Gaussian noise added to the signal current after detection but before processing. The code is available in [26].

2.3. Scalability

The system is scaled by cascading the 2-channel system in a converging tree structure, see Fig. 4(a). Each stage has its own control system and compensates only the relative phase between its two channels of interest. As each stage has its own monitoring port at which the error signal may be tapped the signals of parallel stages are easily separated.

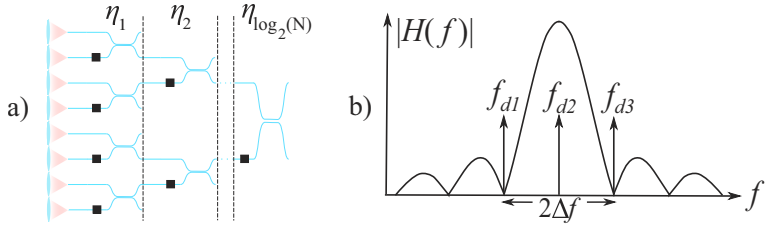

Fig. 4. a) Scaling to $2^k = N$ channels. Each set of parallel stages experience the same external conditions and are therefore assumed to operate at the same combining efficiency. b) The transfer function of the digital bandpass filter of the micro-controller operating at dither frequency f_{d2}. Error signals at different dither frequencies are suppressed by fitting them to the null-points of the sinc-shaped filter.

Optics EXPRESS

Interference between dithers at subsequent stages in the tree is avoided by employing a different frequency for each combining stage. The digital filter in the corresponding micro-controller is adjusted to suppress the dither tones from other combining stages, see Fig. 4(b).

The final combined output power P_c of the entire combining structure is related to the total input power NP_s via the overall N-channel combining efficiency $\eta_N = P_c/NP_s$, where optical excess loss is excluded. The time-average N-channel combining efficiency is related to the combining efficiency of the individual stages as (using sinc ≈ 1 in Eq. (5))

$$\bar{\eta}_N = \prod_{k=1}^{\log_2(N)} \bar{\eta}_k, \quad \bar{\eta}_{j,\max} \approx \frac{1}{2}\left[1 + \prod_{k=1}^{j} J_0\left(\frac{\phi_{\mathrm{mag,k}}}{2^{j-k}}\right)^{(2^{j-k})}\right] \tag{9}$$

where index k denotes the number of each set of parallel stages (for which the dither magnitudes are assumed the same), see Fig. 4(a) and $\bar{\eta}_{j,\max}$ is the maximum efficiency at a stage in the j:th set of parallel stages if separate dither frequencies are used on all stages.

Even though the phase dithers from prior stages are filtered away digitally in later stages, they still reduce the combining efficiency in subsequent stages as they constitute phase variations too fast to compensate. The maximum efficiency at a stage in the j:th set in Eq. (9) provide an approximate expression for this reduced efficiency. If dithers of parallel stages use the same dither frequency and are synchronised in-phase this issue is circumvented and $\bar{\eta}_{j,\max}$ is given by Eq. (5). In this work no in-phase synchronisation was carried out and to avoid interference separate dither frequencies on all three control systems for the 4-channel combining was used.

Practically, a finite insertion loss L_s is present for each stage which implies an additional $L_s^{\log_2(N)}$ total loss (e.g. 2.45 dB for a pessimistic $L_s = 0.35$ dB and $N = 128$) for N channels and an actual combined output power $P_{\mathrm{out}} = N\eta_N P_s/L_s^{\log_2(N)}$.

3. Experimental procedure

To experimentally evaluate the performance of the proposed system the combining efficiency was measured at different received power per aperture P_s as well as at different phase fluctuation strengths $\sigma_{\dot{\phi}}$ and bit error rate (BER) of a combined communications signal was measured.

The scalability was investigated by comparing 2 and 4-channel combining.

3.1. Experimental setup

The experimental setup is presented in Fig. 5.

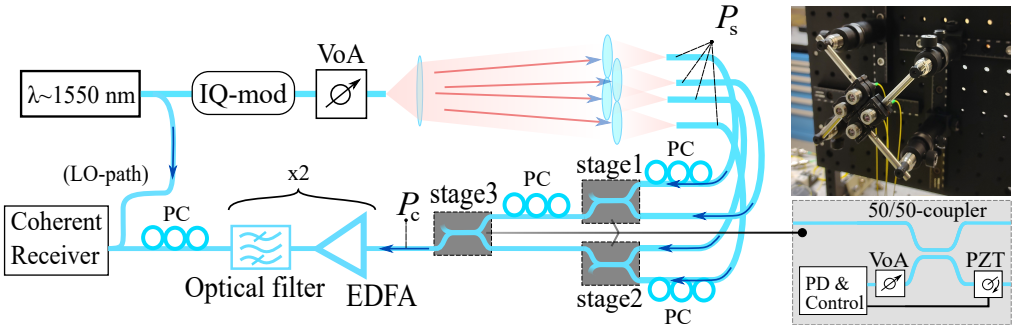

Fig. 5. Left: A schematic of the experimental setup. VoA: variable optical attenuator. Top right: A photo from the setup of the four receive apertures. Bottom right: A single combining stage.

The linearly polarised light from a stable sub-kHz linewidth FBG laser at wavelength $\lambda = 1550.65$ nm was sent through an IQ-modulator and modulated by a 10 Gbaud ($\Delta\nu_{\mathrm{signal}} = 10$GHz)

Optics EXPRESS

non return to zero (NRZ) QPSK signal. The signal was then passed through a variable optical attenuator (VoA) for adjusting the power before being transmitted into free space using a fiber collimator. After about 1 m propagation in free space, four collimators were used to couple the received light into separate SMFs.

The receive collimators were individually aligned to equalize the received optical power between their respective SMF. To ensure equivalent delays between channels for when combining QPSK data the fibers were spliced to within 1 cm and for fine tuning the individual receive aperture positions were adjusted in the direction of propagation. PCs followed by combining stages were adjusted to align the polarisations of the combined channels.

The combined signal P_c was amplified using two cascaded sets of an EDFA followed by an optical filter before coherent homodyne detection and sampling in a real-time oscilloscope. The offline data processing utilized QPSK DSP involving: resampling, IQ-imbalance compensation, frequency offset compensation, CMA and carrier phase estimation as described in [27].

The combining stages (1-3) are the same as in Fig. 2 but with the addition of a VoA before the PD-stage as shown in the bottom right of Fig. 5. To the combining system the action of attenuating the error signal before the PD-stage is equivalent to attenuating the actual received power per aperture. For accurate measurement of the combining efficiency the power received by the apertures was therefore kept constant and P_s, experienced by the control system, was swept using the VoAs prior to the PD-stages. In this way the combining efficiency is directly given by the change in combined power which is kept above the noise floor of the power meters via this approach. To provide taps for the power meters another 50/50-coupler was connected to each of the outputs of the 50/50-coupler of stage 3. The PD-stage is given by Fig. 3 using an optical fiber Bragg grating filter with $\Delta\nu = 0.22$ nm and EDFAs with noise figures $F_n = 3.6 - 4$ dB.

To emulate different strengths of phase fluctuations pseudo random noise was generated in the micro-controllers and added to the compensating voltage signal, thereby inducing phase fluctuations through the PZT: $\phi_{\mathrm{PZT}} = -\phi_{\mathrm{DC}} + \phi_{\mathrm{dither}} + \phi_{\mathrm{excess}}$. This excess phase fluctuation adds to the otherwise slow fluctuation induced by (in-lab) environmental factors, which was characterised to be roughly 8 rad/s, see Supplement 1 sect. 2D.2. When combining four channels three different uncorrelated excess phase fluctuations of the same strength were applied at the three different PZTs. More details regarding the excess and environment-induced fluctuations can be found in Supplement 1 sect. 2D.3.

The time-average combining efficiency $\bar{\eta}$ (written as η from now on) was measured using the above-mentioned taps for power detection where P_1 and P_2 of stage 3 (see Fig. 5 and Fig. 2) are detected using power meters. The 2-channel combining efficiency is then calculated using Eq. (4). During this measurement 2 of the apertures were blocked such that the inputs to stage 3 carried equal power. For 4-channel combining no aperture was blocked and the combining efficiency of stage 3 was measured and then multiplied with the previously measured 2-channel combining efficiency. This gives the 4-channel combining efficiency in accordance with Eq. (9) if combining stages 1 and 2 perform identically to stage 3 during the 2-channel combining. Estimation of uncertainty in measurements is discussed in Supplement 1 sect. 2E.

The dither frequencies for stage 1-3 were $f_{d1} = 20$ kHz, $f_{d2} = 15$ kHz and $f_{d3} = 25$ kHz respectively. The DAC dither update frequency was 8 times the dither frequency, as was the ADC sampling frequency, while the update frequency of the phase compensation (ϕ_{DC}) equaled the dither frequency. The code for the micro-controller can be found in [26] while its main functions are presented in Supplement 1 sect. 2C. The voltage provided by the DAC was amplified using a PZT controller before being fed to the PZTs.

4. Combining efficiency of a single stage

Here we present the results of the single combining stage when subjected to different external conditions and discuss its performance in terms of the combining efficiency. The general

Optics EXPRESS

dependence between combining efficiency and system parameters is briefly mentioned while further details are available in Supplement 1 sect. 3.

Figure 6 shows the measured η_2 vs. P_s for different phase dither modulation magnitudes ϕ_{mag} at an excess fluctuation strength $\sigma_{\dot{\phi}} = 51.3$ rad/s between the channels for both a measured QPSK signal as well as a time domain simulation for comparison. A high combining efficiency is generally maintained until P_s decreases past the system sensitivity and η_2 rapidly drops towards $\eta_2 = 0.5$, corresponding to incoherent combining. Results thereby seem to support the proposed noise-limit criterion $E_{1\text{rad}}/N_0 \geq (E_{1\text{rad}}/N_0)_{\text{thr}}(\eta)$.

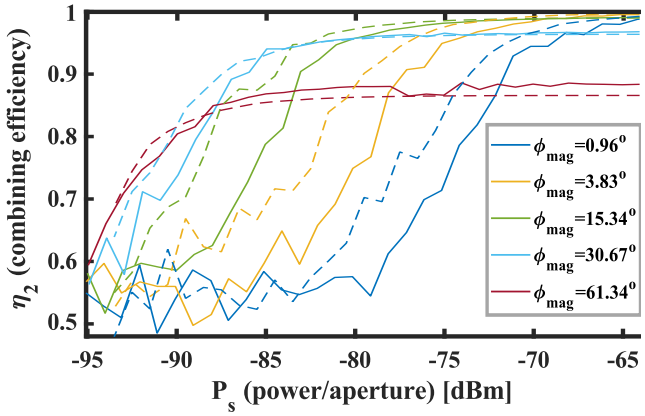

Fig. 6. Measured (solid lines) and simulated (dashed lines) 2-channel combining efficiency vs. received power per aperture for different phase dither modulation magnitudes ϕ_{mag}. The applied excess phase fluctuation strength was $\sigma_{\dot{\phi}} = 51.3$ rad/s and system parameters set to $\Delta f = 5$ kHz, $\phi_{\text{step}} = 1.64°$, $f_{\text{dither}} = 20$ kHz.

Furthermore, we observe how both the system sensitivity and maximum η_2 is altered by different phase dither magnitudes. This is expected as the error signal scales with ϕ_{mag} and much like predicted by Eq. (7) we see about 3dB improvement in sensitivity as ϕ_{mag} is doubled. Results thereby suggests that larger modulation magnitudes can be used to improve sensitivity, however, while also reducing the maximum attainable combining efficiency. This decrease in maximum η_2, observed at different ϕ_{mag}, matches that predicted by Eq. (5). Maximising η_2 at a specific P_s therefore involves selecting the optimal ϕ_{mag}.

Simulations and measurements closely match with a difference in terms of a fixed offset in P_s, where measurement perform slightly worse. This can be attributed to implementation penalties of the system.

Looking instead at the system speed, Fig. 7(a) shows η_2 vs. excess $\sigma_{\dot{\phi}}$ at high P_s for different step sizes. Clearly, larger step sizes allow phase compensation of stronger fluctuations, much in accordance with the speed limit criterion of Eq. (6). Again we see a comparison between simulation and experiment. Moreover, the theoretical maximum $\sigma_{\dot{\phi}}$ the system can handle is $\phi_{\text{step}} \cdot 20$ kHz$/\alpha = 46.6$ rad/s, 93.3 rad/s and 186.6 rad/s for the three investigated step sizes respectively. Here, $\alpha = 2.45$ was used for the emulated phase fluctuations to ensure no speed penalty to η, see Supplement 1 sect. 2D.3. The calculated values match the observed η_2-cut-offs reasonably well. However, according to additional measurement results in Supplement 1 sect. 3, it was found that larger step sizes were optimal w.r.t. the system sensitivity (although not by much) despite it decreasing the $E_{1\text{rad}}/N_0$. As the error SNR decreases with lower P_s the effective step size decreases, $\phi_{\text{eff-step}} = \phi_{\text{step}}\text{SNR}/(1 + \text{SNR})$, as occasional steps are taken in the wrong direction due to noise. This is likely the cause for larger step-sizes being optimal at lower P_s. The optimised step size at $\sigma_{\dot{\phi}} = 51.3$ rad/s for minimised sensitivity was $\phi_{\text{step}} = 1.64°$ for instance.

Optics EXPRESS

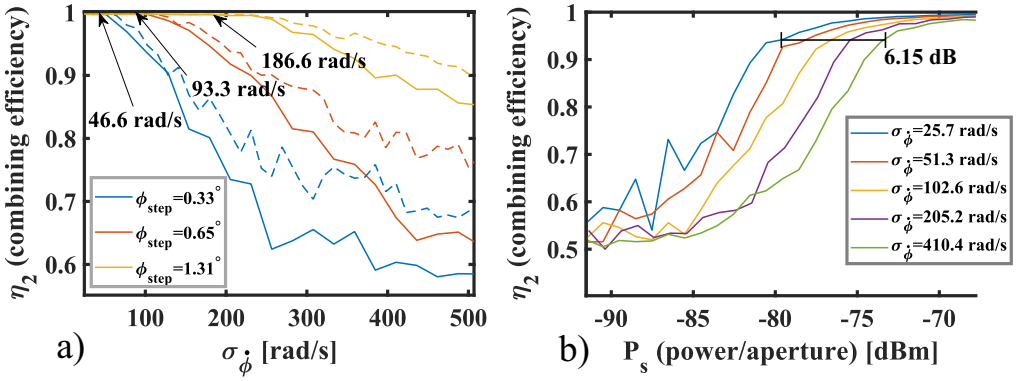

Fig. 7. a) Measured 2-channel combining efficiency vs. excess fluctuation strength for different step sizes ϕ_{step}, where $P_s = -48.7$ dBm, $\phi_{\text{mag}} = 7.67°$, $\Delta f = 5$ kHz and $f_{\text{dither}} = 20$ kHz. b) Measured 2-channel combining efficiency vs. received power per aperture for different excess fluctuation strengths $\sigma_{\dot{\phi}}$, with $\phi_{\text{mag}} = 7.67°$, $\Delta f = 5$ kHz and $f_{\text{dither}} = 20$ kHz. For each respective fluctuation case the step size was optimised, values from blue to green: $\phi_{\text{step}} = [0.98°, 1.64°, 2.29°, 2.62°, 3.93°]$.

Next, Fig. 7(b) shows the measured η_2 vs P_s at different excess fluctuation strengths $\sigma_{\dot{\phi}}$. Between each fluctuation case the step size was optimised to minimise the sensitivity. The results show how the sensitivity of the system (at 95% η) is increased by about 1.5 dB per doubling of fluctuation strength, this in accordance with the criterion of Eq. (8) ($\eta = \text{const} \implies P_s^2 \propto \sigma_{\dot{\phi}} \Delta\nu_s$).

It can be useful to analyse the combining efficiency w.r.t. its penalties due to system parameters and external conditions (see sect. 2.1) respectively: $\eta = \eta_{\text{system}}\eta_{\text{external}}$. While η_{system} sets the maximum limit of η_2 in the presented results, η_{external} accounts for the change in η as it decays from close to 100% efficiency at high P_s and low $\sigma_{\dot{\phi}}$ toward 50% at low P_s and high $\sigma_{\dot{\phi}}$. We allow reduction in η_{system} as long as the gain in η_{external} is higher, resulting in a higher η.

Apart from the system parameters ϕ_{mag} and ϕ_{step}, the bandwidth of the digital bandpass filter Δf as well as the dither frequency f_{dither} need to be selected. The dither frequency sets a maximum limit to the system speed and might require an increase at stronger fluctuations. It is however practically limited by the frequency-response of the PZT (including controller) and furthermore by available frequency spacing when using multiple dithers for multi-channel combining. If step-size and dither frequency are altered while keeping $\phi_{\text{step}} f_{\text{dither}} = 1/t_{1\text{rad}}$ constant (and $\phi_{\text{step}} \ll \pi$) the system performance is maintained as verified by measurements.

While the filter bandwidth Δf must be large enough to accommodate the bandwidth of the phase fluctuation, it primarily limits the system in terms of its equivalent loop delay. The reduced efficiency predicted by Eq. (5) at small Δf together with the condition of Eq. (6) shows that the strength of phase fluctuations $\sigma_{\dot{\phi}}$ constrain Δf, i.e., the minimum dither spacing for multi-channel combining. As such, the choice of both Δf and f_{dither} are restricted by $\sigma_{\dot{\phi}}$, the number of channels to combine and the maximum dither frequency the system can support.

While not presented here, our measurements confirm combining of QPSK data and a continuous wave (CW) signal performs the same in terms of combining efficiency.

4.1. Generalised 2-channel combining efficiency

With complete control over the system parameters, assuming that they are always optimised we are interested to know the maximum η the system can achieve. This best attainable combining efficiency is a function of the variables external to the system: $\eta_{\max}(P_s, \sigma_{\dot{\phi}}, \Delta\nu_{\text{signal}})$. The combined requirement in Eq. (8) states that system performance is maintained as long as

Optics EXPRESS

$P_s^2/\sigma_{\dot{\phi}}\Delta\nu_{\text{signal}}$ is maintained. As results support the criterion in Eq. (8) we use this fact and the measured and simulated curves of Fig. 6, representing maximal η at $\sigma_{\dot{\phi}} = 51.3$ rad/s, $\Delta\nu = 27.5$ GHz and different P_s to construct a prediction of $\eta_{\max}$. It is obtained by drawing a line enclosing the outermost boundaries of the curves in Fig. 6 and is presented in Fig. 8.

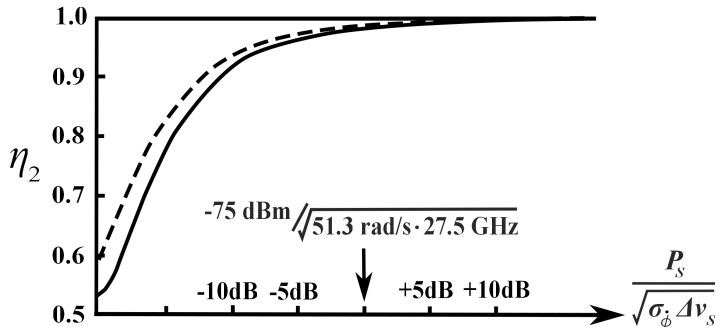

Fig. 8. The estimated maximum combining efficiency possible for 2 channels as function of the optical signal bandwidth $\Delta\nu_s$, the average optical signal power per aperture P_s and the phase fluctuation strength $\sigma_{\dot{\phi}}$. The estimation is based on the experiment (solid line) and simulation (dashed line) presented in Fig. 6.

The result in Fig. 8 provides a general prediction of the achievable 2-channel combining efficiency η_2 as a function of P_s, $\sigma_{\dot{\phi}}$ and $\Delta\nu_s$. It can be a useful estimation to rely on when designing the receiver unit, considering aperture sizes etc.

5. Combining efficiency of an N-channel combining structure

Here we discuss the N-channel combining efficiency η_N for more than two channels. First we will compare the 2 and 4-channel results in light of the theoretical prediction of Eq. (9).

A comparison between measurements of η_2 and η_4 with excess $\sigma_{\dot{\phi}} = 51.3$ rad/s and without excess phase fluctuations is presented in Fig. 9(a) in terms of combining efficiency and in Fig. 9(b) in terms of BER. Note that P_s is the power per aperture experienced by the control system and not by the coherent receiver which received a power $P_r = \eta_4(P_s)P_0$, where $P_0 = -46.9$ dBm. The system parameters for each stage were optimised for maximum combining efficiency at $P_s = -80$ dBm and at $P_s = -70$ dBm without and with excess phase fluctuations respectively.

Comparing the combining efficiencies between 2 and 4 channels at the powers per aperture the two respective cases are optimised for, we have: at -70 dBm $\eta_2 = 0.991$ which goes to $\eta_4 = 0.984$ (orange) and at -80 dBm $\eta_2 = 0.985$ to $\eta_4 = 0.969$ (blue) as indicated in the figure. The measured results compare reasonably well with the theoretically estimated 4-channel combining efficiencies $\eta_4 = 0.991^2 = 0.982$ (orange) and $\eta_4 = 0.985^2 = 0.970$ (blue), based on Eq. (9), the measured η_2 and the assumption of identical performance across all combining stages. The positive difference between measured and calculated η_4 for the orange case is likely due to an increase in η_{external} being larger than the decrease in η_{system}. The opposite would explain the negative difference in the blue case, especially as its dither magnitude is twice as large.

Looking instead at the signal quality, comparing Fig. 9(a) and (b) shows that the increase in BER stems directly from the decrease in measured η_4. For optical bandwidths as narrow as that investigated here, there is no significant dispersion nor influence of the PZT wavelength-dependent phase-change that would affect the signal. The phase modulation on the combined signal ($\leq \phi_{\text{mag}}/2$) due to the known dithers is likely negligible in relation to practical laser phase noise. It can, however, be accounted for in the DSP and will, if not, be compensated by the carrier-phase estimation. Thus the main parameter affected by the system is the power transmittance and as such the combining efficiency alone governs the change in BER. This result

Optics EXPRESS

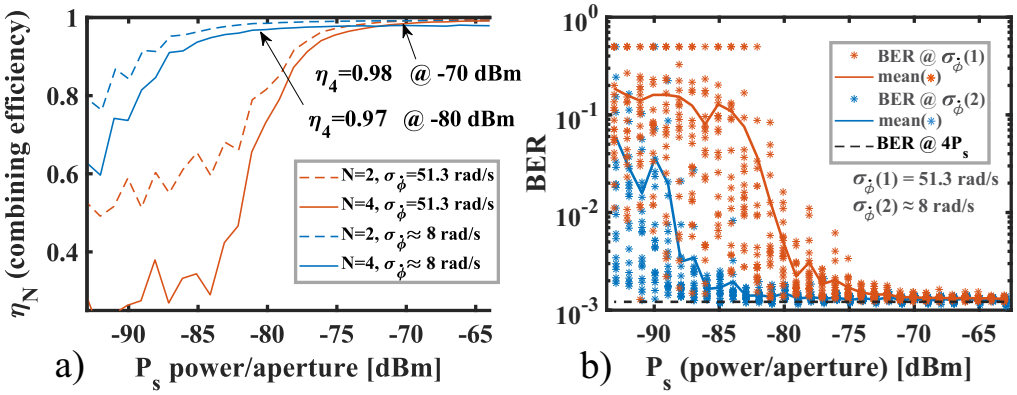

Fig. 9. a) Measured η_2 (dashed lines) and η_4 (solid lines) vs. P_s. Orange curves are with $\sigma_{\dot\phi}$ = 51.3 rad/s, blue curves are without excess fluctuations. b) Measured BER of the 4-channel combining measurement in a) for matching colors. The dashed black line represents BER at η_4 = 1 (received power of −46.9 dBm). System parameters: $\phi_{\text{mag}} = 7.67°$, Δf = 5 kHz, $\phi_{\text{step}} = [1.64°, 2.29°, 1.31°]$ for stage 1-3 respectively (orange) and $\phi_{\text{mag}} = 15.34°$, Δf = 2.5 kHz, $\phi_{\text{step}} = [0.20°, 0.29°, 0.16°]$ (blue).

indicates that η_N is enough to describe the combining operation on any type of optical signal, as long as dispersion is negligible and path lengths are matched in respect to the signal bandwidth.

As the evolution from η_2 to η_4 matches theoretical predictions we can use this to extrapolate to larger N. Calculating η_N from η_2 in Fig. 9(a) at the indicated powers (P_s) leads to the results in Fig. 10. Figure 10 compares the simple estimate assuming identical performance for all stages $\eta_N = \eta_2^{\log_2(N)}$ (solid), the measured points from Fig. 9 as well as a pessimistic prediction that takes into account the reduced efficiency due to multiple dithers (dashed).

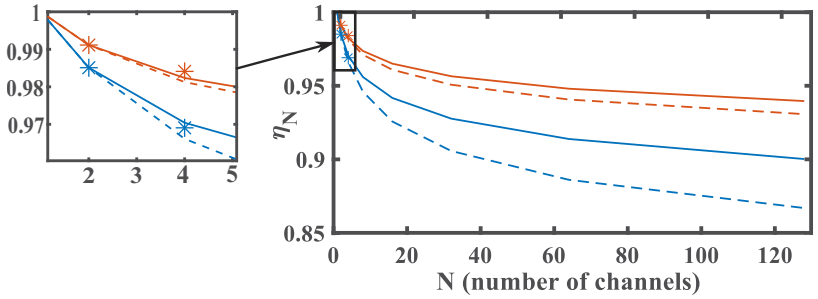

Fig. 10. Evolution of the total combining efficiency η_N as the number of channels N increase. Stars are the measured η_2 and η_4 of Fig. 9(a) at the indicated P_s of the respective colors (blue: no excess fluctuations at P_s = −80 dBm and orange: $\sigma_{\dot\phi}$ = 51.3 rad/s at P_s = −70 dBm). Solid lines are calculated from the measured η_2 (both cases) using $\eta_N = \eta_2^{\log_2(N)}$ and dashed lines are calculated using Eq. (9) by first separating $\eta_2 = \eta_{\text{system}}\eta_{\text{external}}$ and update η_{system} according to Eq. (9) (using the given maximum efficiency per stage) while keeping η_{external} constant. This is a pessimistic prediction as η_{external} is expected to increase as the combined power increases with each stage.

The simple estimate of Fig. 10 matches measured values and predict $\eta_{128} = 0.991^7 = 0.939$ and $\eta_{128} = 0.985^7 = 0.900$ for the case of with and without excess fluctuations at −70 and −80 dBm respectively. This corresponds to a loss of 0.27 and 0.46 dB respectively and a total combining gain of $N\eta_N = 128\eta_{128} = 20.8$ and 20.6 dB respectively from the combining structure.

Optics EXPRESS

Even the pessimistic estimate, which serves as a lower limit of the prediction, suggests a loss of 0.32 dB and 0.62 dB for the two respective cases. A 128-aperture combining structure capturing −70 dBm of power per aperture would then produce a signal output power of about −50 dBm minus 1-2 dB of waveguide and component losses.

These predictions are possible to improve further. If we instead use identical phase dithers at parallel stages, synchronised in-phase, then the solid lines of Fig. 10 would constitute the lower bound of η_N. This also means only needing $\log_2(N)$ separate dither tones which may be a necessity at large N to fit all dithers in the available PZT bandwidth. Moreover, as the power is increased with each stage the external condition changes for later stages. This can be exploited by decreasing e.g. ϕ_{mag} as power increases to allow higher η_{system} (refer to Eq. (5)) if the penalty to η_{external} (refer to Eq. (7)) is negligible by doing so.

However, while the power increases for later stages, $\sigma_{\dot{\phi}}$ may increase depending on aperture separation and spatial coherence of the received wave. If the fluctuation for instance is caused by angle of arrival fluctuations then the fluctuation strength is proportional to aperture separation and as a result the phase fluctuations will grow stronger between channels combined in later stages. By carefully choosing which channels are modulated by the PZT, the spatial decorrelation at larger aperture separations can be compensated partially. The maximum η_N possible for the system will therefore depend on the characteristics of the free-space link and the geometry of the combining structure, i.e. which channels are compensated by the PZT and which apertures are combined and when in the converging tree structure. This investigation is beyond the scope of this study but is unlikely to result in worse combining efficiencies than predicted by Fig. 10 if carried out sensibly. Recall that even if both P_s and $\sigma_{\dot{\phi}}$ is doubled by each stage the criterion of Eq. (8) is relaxed and performance can be improved.

To summarise, Fig. 10 provides a reasonable estimate of η_N with potential improvement possible depending on the channel properties. Using Fig. 10 together with Fig. 8 we are therefore able to estimate η_N for different external conditions as well as for a larger number of channels.

6. Discussion and conclusion

Analog combining of low per-aperture optical power (P_s) under different phase fluctuation strengths has been investigated. Key to the approach is the optical preamplification of low signal powers ($P_s < -61\text{dBm}/(1-\eta) \approx -43\text{dBm}$) for which the ASE self-beat noise dominates in error signal reception. We have demonstrated coherent combining of as low as −80dBm optical power per aperture in a stable lab environment with an efficiency of 97% for 4 channels of 10 Gbaud QPSK data. Under phase fluctuations with a standard deviation of $\sigma_{\dot{\phi}} = 51.3$ rad/s an efficiency of 98% was obtained at −70dBm power per aperture.

We have presented a theory which further supports the results. An estimate of system performance in terms of the best possible combining efficiency was constructed. The estimate considers the important external parameters: input optical signal power per aperture, optical signal bandwidth, phase fluctuation strength and the number of combined channels. The estimate relates the combining efficiency to these parameters and may be a useful tool for performance prediction and design of combining systems when the received optical signal power is low. Generally, higher received powers are required to operate the control system efficiently when either phase fluctuations are severe or the optical signal bandwidth is large.

For applications where it is possible to meet both the noise and bandwidth limit criteria this system is able to provide high combining efficiencies of several tens of GHz optical bandwidth signals. This implies a significantly higher data rate compared to the, often bandwidth-limited cooled detector approaches such as those studied in [7]. Moreover, if the optical fiber-based combining stages can be re-designed onto a chip-based platform, where PZTs are exchanged by thermo-optic heaters, the system size and losses can be made minimal. In addition, the

Optics EXPRESS

environmental-induced phase fluctuations are expected to be much smaller for a shorter and more confined system which would allow combining at even lower powers than demonstrated here.

Comparing the presented system with digital approaches is non-trivial but considering the discussions in [22] there are apparent limitations to digital combining in terms of computational complexity for achieving both real-time operation as well as high combining efficiencies. In fact, [22] propose a combining loss of 0.5 dB as trade-off to achieve real-time operation for combining of at least four −10 dB optical signal to noise ratio (OSNR) per-aperture signals ($P_s \approx -68$ dBm) with a symbol rate of 10 Gbaud and no applied phase fluctuations. Meanwhile for our system we predict an intrinsic combining loss of 0.46-0.62 dB for $N = 128$ channels at −80 dBm received power per aperture at the same symbol rate using $N - 1$ relatively inexpensive error feedback loops as opposed to the extra $N - 1$ coherent receivers needed for digital combining.

The analog combining system also provides a combined optical signal which is available for further optical processing. On the downside, in case of a combining stage failure the impact on the overall combining efficiency is larger in the analog approach. The efficiency loss is larger the further into the combining tree-structure a stage breaks with a maximum of 3dB for the final stage with rapidly decreasing penalty towards the outermost stages with loss $-10\log_{10}[(N-1)/N]$ dB as for the digital system. Implementing a polariser in the power detection stage of the analog system may also be practically difficult as it requires absolute control of polarisation compared to the relative control required between channels for coherent combining. Without it the noise power is doubled and the curve in Fig. 8 is shifted 1.5 dB to the right, reducing the sensitivity by the same amount. Significant amplitude fluctuations present between receive apertures will also degrade the combining efficiency as well as the system sensitivity, although at relatively moderate amounts (efficiency > 0.9 and sensitivity decrease < 1 dB for power ratios < 6 dB). In case strong amplitude fluctuations manifest, e.g. in turbulent atmospheric channels a Mach-Zenhder interferometer can be added for compensation of both phase and amplitude, as in [28].

The investigated analog system may prove interesting where SNR, cost and complexity is of concern, such as in deep space-to-earth communications.

Funding. Vetenskapsrådet (VR-2015-00535).

Acknowledgments. Portions of this work were presented at OFC in 2022, Coherent Combining at Ultra-low Optical Signal Powers based on Optically Amplified Error Feedback. For providing interesting and encouraging conversations I would like to thank my colleagues at the photonics lab at Chalmers department of michrotechnology and nanoscience. I wish to also thank Ali Mirani, Zonglong He and last but not least Kovendhan Viyajan for assisting with occasional troubleshooting as well as for providing helpful advice and help in the lab.

Disclosures. The authors declare no conflicts of interest.

Data availability. Data underlying the results presented in this paper are available in [26].

Supplemental document. See Supplement 1 for supporting content.

References

1. H. Hemmati and D. Caplan, "Optical Satellite Communications," in *Optical Fiber Telecommunications Volume VIB: Systems and Networks* (Elsevier, 2013), pp. 121–162.
2. M. Toyoshima, W. R. Leeb, H. Kunimori, and T. Takano, "Comparison of microwave and light wave communication systems in space applications," Opt. Eng. **46**, 1–7 (2007).
3. P. Hopman, P. Boettcher, L. Candell, J. Glettler, R. Shoup, and G. Zogbi, "An end-to-end demonstration of a receiver array based free-space photon counting communications link," Proc. SPIE **6304**, 63040H (2006).
4. D. Boroson, B. Robinson, D. Burianek, D. Murphy, and A. Biswas, "Overview and status of the lunar laser communications demonstration," Proc. SPIE **8246**, 82460C (2012).
5. D. Caplan, "Laser communication transmitter and receiver design," J. Opt. Commun. Rep. **4**(4-5), 225–362 (2007).
6. D. M. Boroson, B. S. Robinson, D. V. Murphy, D. A. Burianek, F. Khatri, J. M. Kovalik, Z. Sodnik, and D. M. Cornwell, "Overview and results of the Lunar Laser Communication Demonstration," in *Free-Space Laser Communication and Atmospheric Propagation XXVI*, vol. 8971 H. Hemmati and D. M. Boroson, eds., International Society for Optics and Photonics (SPIE, 2014), pp. 213–223.
7. B. S. Robinson, A. J. Kerman, E. A. Dauler, R. J. Barron, D. O. Caplan, M. L. Stevens, J. J. Carney, S. A. Hamilton, J. K. Yang, and K. K. Berggren, "781 mbit/s photon-counting optical communications using a superconducting nanowire detector," Opt. Lett. **31**(4), 444–446 (2006).

Optics EXPRESS

8. C. Zhang, K. Uyama, Z. Zhang, L. Jin, S. Y. Set, and S. Yamashita, "Recent trends in coherent free-space optical communications," in *Metro and Data Center Optical Networks and Short-Reach Links IV*, vol. 11712 A. K. Srivastava, M. Glick, and Y. Akasaka, eds., International Society for Optics and Photonics (SPIE, 2021), pp. 96–109.
9. W. Liu, K. Yao, D. Huang, X. Lin, L. Wang, and Y. Lv, "Performance evaluation of coherent free space optical communications with a double-stage fast-steering-mirror adaptive optics system depending on the greenwood frequency," Opt. Express **24**(12), 13288–13302 (2016).
10. C. Liu, M. Chen, S. Chen, and H. Xian, "Adaptive optics for the free-space coherent optical communications," Opt. Commun. **361**, 21–24 (2016).
11. J. Cao, X. Zhao, W. Liu, and H. Gu, "Performance analysis of a coherent free space optical communication system based on experiment," Opt. Express **25**(13), 15299–15312 (2017).
12. H. P. Stahl, "Survey of cost models for space telescopes," Opt. Eng. **49**(5), 053005 (2010).
13. J. Park, E. Lee, C.-B. Chae, and G. Yoon, "Performance analysis of coherent free-space optical systems with multiple receivers," IEEE Photonics Technol. Lett. **27**(9), 1010–1013 (2015).
14. Y. Bian, Y. Li, D. Zheng, T. Dong, E. Chen, W. Li, X. Hong, J. Qiu, Y. Jie, Y. Su, and J. Wu, "Performance investigation of satellite-to-ground downlink optical communications employing aperture diversity combined with mode diversity," Opt. Commun. **491**, 126958 (2021).
15. Y. Yang, C. Geng, F. Li, G. Huang, and X. Li, "Multi-aperture all-fiber active coherent beam combining for free-space optical communication receivers," Opt. Express **25**(22), 27519–27532 (2017).
16. C. Geng, F. Li, J. Zuo, J. Liu, X. Yang, T. Yu, J. Jiang, and X. Li, "Fiber laser transceiving and wavefront aberration mitigation with adaptive distributed aperture array for free-space optical communications," Opt. Lett. **45**(7), 1906–1909 (2020).
17. C. Lao, J. Sun, Z. Lu, J. Li, M. Xu, H. He, R. Han, X. Cai, and Y. Li, "Multi-aperture fiber coherent combining system in urban horizontal atmospheric laser link," Opt. Commun. **466**, 125172 (2020).
18. A. Limery, L. Lombard, P. Bourdon, A. Billaud, O. Pinel, G. Labroille, T. L. Guennic, and P. Jian, "Coherent combining of 7 fiber lasers using a multi-plane light converter device," in *Technologies for Optical Countermeasures XVIII and High-Power Lasers: Technology and Systems, Platforms, Effects V*, vol. 11867 D. H. Titterton, R. J. Grasso, M. A. Richardson, W. L. Bohn, and H. Ackermann, eds., International Society for Optics and Photonics (SPIE, 2021), pp. 95–101.
19. R. Kakarla, J. Schröder, and P. A. Andrekson, "One photon-per-bit receiver using near-noiseless phase-sensitive amplification," Light: Sci. Appl. **9**(1), 153 (2020).
20. D. J. Geisler, T. M. Yarnall, M. L. Stevens, C. M. Schieler, B. S. Robinson, and S. A. Hamilton, "Multi-aperture digital coherent combining for free-space optical communication receivers," Opt. Express **24**(12), 12661–12671 (2016).
21. Y. Tu, S. Cui, K. Zhou, and D. Liu, "Phase alignment with minimum complexity for equal gain combining in multi-aperture free-space digital coherent optical communication receivers," IEEE Photonics J. **12**(2), 1–10 (2020).
22. C. Rao, S. Cui, Y. Tu, K. Zhou, and D. Liu, "Toward practical digital phase alignment for coherent beam combining in multi-aperture free space coherent optical receivers," IEEE Access **8**, 202585–202595 (2020).
23. J. Sun, P. Huang, Z. Yao, and J. Guo, "Adaptive digital combining for coherent free space optical communications with spatial diversity reception," Opt. Commun. **444**, 32–38 (2019).
24. M. R. Garcia-Talavera, S. Chueca, A. Alonso, T. Viera, and Z. Sodnik, "Analysis of the preliminary optical links between ARTEMIS and the Optical Ground Station," in *Free-Space Laser Communication and Laser Imaging II*, vol. 4821 J. C. Ricklin and D. G. Voelz, eds., International Society for Optics and Photonics (SPIE, 2002), pp. 33–43.
25. G. Agrawal, *Fiber-Optic Communication Systems* (Wiley, 2021).
26. R. Larsson, J. Schröder, M. Karlsson, and P. Andrekson, "Data - Coherent combining of low-power optical signals based on optically amplified error feedback," Zenodo (2022), https://doi.org/10.5281/zenodo.5796219.
27. S. J. Savory, "Digital filters for coherent optical receivers," Opt. Express **16**(2), 804–817 (2008).
28. V. Billault, J. Bourderionnet, J. P. Mazellier, L. Leviandier, P. Feneyrou, A. Maho, M. Sotom, X. Normandin, H. Lonjaret, and A. Brignon, "Free space optical communication receiver based on a spatial demultiplexer and a photonic integrated coherent combining circuit," Opt. Express **29**(21), 33134–33143 (2021).